https://doi.org/10.48048/tis.2022.6314

Radiative MHD Non-Newtonian Chemically Reactive Nanofluid Flow with Heat Source Induced by Non-linear Stretching Cylinder

Vinita Makkar[1,*], Vikas Poply[2] and Naresh Sharma[1]

[1]Department of Basic and Applied Sciences, GD Goenka University, Haryana 122103, India
[2]Department of Mathematics, KLP College Rewari, Haryana 123401, India

([*]Corresponding author's e-mail: vini252011makkar@gmail.com)

Received: 14 August 2021, Revised: 8 October 2021, Accepted: 15 October 2021, Published: 31 October 2022

Abstract

Magnetohydrodynamic (MHD) chemically reacting flow by Casson nanofluid bounded by a stretched surface is analyzed. Convective conditions of transport phenomena, radiation and heat generation /absorption effects are discussed. Influence of Brownian motion and thermophoresis has been taken into account. This manuscript investigates the outcomes of yield stress, thermophoresis, Brownian motion, magnetic parameter, Prandtl number, radiation parameter and thermal conductivity on velocity, temperature and nanoparticle concentration profiles. To solve transformed equations, a well designed numerical technique (Runge Kutta Fehlberg) has been implemented by following Shooting procedure. MATLAB programming with ODE45 solver is used to calculate results and compare for local Nusselt number ($-\theta_\alpha'(0)$) with extant outcomes in the absence of nanofluid parameters via table and bar graphs for pertinent values of Prandtl number and non linear stretching parameter. An excellent agreement is noted for linear and non-linear stretching cylinder. The impact of controlling fluid parameters is represented graphically. Additionally, physical quantities of interest are tabulated and explained via graphs.

Keywords: Casson nanofluid, Buongiorno's model, MHD flow, Chemical reaction, Heat radiation

Introduction

A rapid progress has urged researcher's attention over flow regime towards stretched cylinder. Stream by a directly or non-straightly extending chamber assumes a critical part and have immense applications in assembling and creation measures including metal turning, creation of glass filaments, elastic sheet creation, wire drawing, expulsion of polymer sheets, oil businesses, polymer handling and so on**.** The flow of quiescent fluid over a moving surface was first analyzed by Sakiadis [1]. He described the application of the boundary layer in a continuous solid environment and incorporated both direct and indirect research methods into his study. Crane [2] has taken the initiative to focus on a straightforward 2-D fixed flow solution with viscous and insoluble fluid over the expanded surface in its aircraft with the same speed due to the same pressure. Nanofluid is an assortment of nanoparticles **(**$10^{-9} - 10^{-7}$m**)** and base liquid that is another idea in the pace of move of warmth. Accordingly, nanofluid upgrades warm conductivity and turns into a particular space of examination and mechanical field specifically, coolants, microelectronics, homegrown fridges, energy units and so on. Since most recent twenty years, the investigation of nanofluid has encouraged the analyst's consideration because of their warmth transmission rate. The term nanofluid was initially generated by Choi and Eastman [3]. Nanofluids heat transportation intensification was thought by Xuan and Li [4] for determination of transportation phenomena by implementation of hot wire procedure**.** Henceforth, Buongiorno [5] clarified the further evolved depiction of nanofluid convection behavior by perceiving Nb and Nt impact**.** Afterthat, Kuznetsov and Nield [6] presented the convective transport in uniform nanofluid layer by following Buongiorno's model. Nadeem *et al.* [7] inspected the stagnation point Casson nanofluid flow towards an extended sheet and affirmed that nanofluid is viewed as a compelling specialist to control temperatures. As of late, different angles on the pace of nanofluid transportation qualities are dissected by various researchers in [8-12].

Recently, the MHD has gained attention due because of controllable rate of heat transportation. MHD conditions over the stretched sheet focus on the quality of several of its applications in research

such as cooling reactors, paper production, petroleum production, glass production, power generator, crude oil refining geophysics, blood flow rate, plasma welding, MHD pump, oil extraction and processing metals, plasma studies etc. The impacts of MHD are useful in clinical field also that is, therapy of tumors or disease and so forth. It is additionally utilized in salt water and fluid metal, which goes about as an electrical directing liquid. Magnetohydrodynamic identification **(**MHD**)** has been utilized to control the speed liquid, which assumes a significant part in an alternate field. Abel and Mahesha [13] analyzed the radiation impact with variable thermal conductivity over stretching surface in presence of MHD flow by following perturbation technique. Hayat *et al*. [14] examined MHD stream transportation by thinking about extended surfaces**.** Vinita and Poply [15] talked about the impact of slip stream with external speed in presence of hydromagnetic nanofluid towards an extended chamber. Salahuddin *et al*. [16] investigated the slip flow by employing FD technique over stretching cylinder in presence of Carreau nanofluids. Recently impact of MHD $AgAg/H_2OO$ nanofluid flow with slip effects induced by stretching surface has been investigated by Mishra and Kumar [17]. Moreover, non-direct effect towards extending surface under various viable conditions has been inspected by the specialists in [18-25].

The yield stress model restricted as a subsection of non-Newtonian fluid that has various utilizations in bioengineering operations, metallalurgy, food processing, etc. In 1959, Casson fluid model was pioneered by Casson [26] for prognosis pigment-oil intermission flow. Furthermore, Casson nanofluid boundary layer fluid flow over disparate geometries was pre-mediated by numerous researchers in [27-30]. Fluid behaves as a solid, if the yield stress is more than applied shear stress. On the other hand, fluid behaves as a liquid for lesser yield stress. Kameshwaran *et al*. [31] investigated the dual solution in shrinking/stretching surface. Flow by Casson fluid against Lorentz force is discussed. Khan *et al*. [32] examined result of gooey dissemination on MHD nanofluid stream past an extending sheet. Afify [33] examined impact of incomplete slip synthetic response and gooey dispersal for Casson nanofluid stream by thinking about extended sheet. Spurred by the above productive examinations done by different analysts and boundless mechanical just as designing applications, we are thus having an expect to unfurl meaning of mass, warmth and stream transportation of MHD Casson liquid past a non-straight extending chamber with substance response. An exact audit of effectively distributed papers concedes that no such investigation has been done as such far. Actual angles, marvel and fruitfulness of musings are featured.

Materials and methods

In current study, radiative MHD incompressible Casson nanofluid flow towards linear/non-linear stretched cylinder is considered as illustrated via **Figure 1**. In this configuration, cylinder is stretched with stretching velocity $u_w = cx^n / L,$ where c denotes a constant, x denotes stretching surface coordinate, n is the stretching parameter with $n=1$ corresponding to linear stretching parameter, $n\neq 1$ corresponds to non-linear stretching parameter and L is the characteristics length. Modeled equations are:

$$\frac{\partial}{\partial x}(ru)+\frac{\partial}{\partial r}(rv)=0, \tag{1}$$

$$u\frac{\partial u}{\partial x}+v\frac{\partial u}{\partial r}=\nu\left(1+\frac{1}{\beta}\right)\left(\frac{\partial^2 u}{\partial r^2}+\frac{1}{r}\frac{\partial u}{\partial r}\right)-\frac{\sigma {B_0}^2}{\rho}u, \tag{2}$$

$$u\frac{\partial T}{\partial x}+v\frac{\partial T}{\partial r}=\alpha\left(\frac{\partial^2 T}{\partial r^2}+\frac{1}{r}\frac{\partial T}{\partial r}\right)+\frac{Q_0}{(\rho c)_f}(T-T_\infty)-\frac{1}{(\rho c)_f}\frac{1}{r}\frac{\partial}{\partial r}(rq_r)+\tau\left[D_B\frac{\partial C}{\partial r}\frac{\partial T}{\partial r}+\frac{D_T}{T_\infty}\left(\frac{\partial T}{\partial r}\right)^2\right] \tag{3}$$

$$u\frac{\partial C}{\partial x}+v\frac{\partial C}{\partial r}=D_B\left(\frac{\partial^2 C}{\partial r^2}+\frac{1}{r}\frac{\partial C}{\partial r}\right)+\frac{D_T}{T_\infty}\left(\frac{\partial^2 T}{\partial r^2}+\frac{1}{r}\frac{\partial T}{\partial r}\right)-\alpha_1\left(C-C_\infty\right),$$

Here vertical and horizontal velocities are represented by v and u, respectively. Also $\alpha = \frac{k_m}{(\rho c)_f}$ depicts the thermal diffusivity, $\tau = \frac{(\rho c)_p}{(\rho c)_f}$ defines a proportion of heat capacities, β denotes Casson fluid parameter, D_T reflects thermophoretic diffusion coefficient, B_0 shows the intensity of magnetic field, ν denotes kinematic viscosity, D_B denotes Brownian diffusion coefficient, σ represents electrical conductivity. Next, C denotes nanoparticle concentration and T is the temperature**.** The relevant B.C's are [34]:

$$u = u_w(x), \quad v = 0, \quad -k\frac{\partial T}{\partial r} = h_f\left(T_f - T\right), \quad -D_m\frac{\partial C}{\partial r} = k_m\left(C_f - C\right) \quad at \quad r = R,$$
$$u \to 0, \quad T \to T_\infty, \quad C \to C_\infty \quad as \quad r \to \infty$$

in which h_f and k_m being the constant convective heat and mass transfer coefficients.

Using similarity variables:

$$\xi = \frac{r^2 - R^2}{2R}\left(\frac{c}{\nu L}\right)^{\frac{1}{2}}, \quad \psi = \left(\frac{\nu c}{L}\right)^{\frac{1}{2}} xRf_\alpha(\xi), \quad \theta_\alpha(\xi) = \frac{T - T_\infty}{T_f - T_\infty}, \quad \phi_\alpha(\xi) = \frac{C - C_\infty}{C_w - C_\infty}$$

in which stream function described by $u = r^{-1}\partial\psi/\partial r$ and $v = -r^{-1}\partial\psi/\partial x$ satisfied (1). By Roseland approximation, we have:

$$q_r \approx -\frac{16\sigma^* T_\infty^3}{3k^*}\frac{\partial T}{\partial r} \tag{1}$$

Here k^* and σ^* stands for mean absorption coefficient and Stefan Boltzmann constant serially. After using (6) and (7), transformed nonlinear ordinary differential equations are:

$$\left(1 + \frac{1}{\beta}\right)\left[\left(1 + 2\xi\gamma\right) f_\alpha''' + 2\gamma f_\alpha''\right] + \left(\frac{n+1}{2}\right) f_\alpha f_\alpha'' - n f_\alpha'^2 - M f_\alpha' = 0 \tag{2}$$

$$(1 + 2\xi\gamma)\left(1 + \frac{4}{3}Rd\right)\theta_\alpha'' + Pr\left[Nb(1 + 2\xi\gamma)\theta_\alpha'\phi_\alpha' + Nt(1 + 2\xi\gamma)\theta_\alpha'^2 + Q\theta_\alpha\right] + \left[2\gamma\left(1 + \frac{4}{3}Rd\right) + Pr\left(\frac{n+1}{2}\right) f_\alpha\right]\theta_\alpha' = 0 \tag{3}$$

$$\left(1 + 2\xi\gamma\right)\phi_\alpha'' + \left(\frac{n+1}{2}\right) LePr f_\alpha\phi_\alpha' + 2\gamma\phi_\alpha' + \left(1 + 2\xi\gamma\right)\frac{Nt}{Nb}\theta_\alpha'' + 2\gamma\frac{Nt}{Nb}\theta_\alpha' - LePrA\phi_\alpha = 0 \tag{4}$$

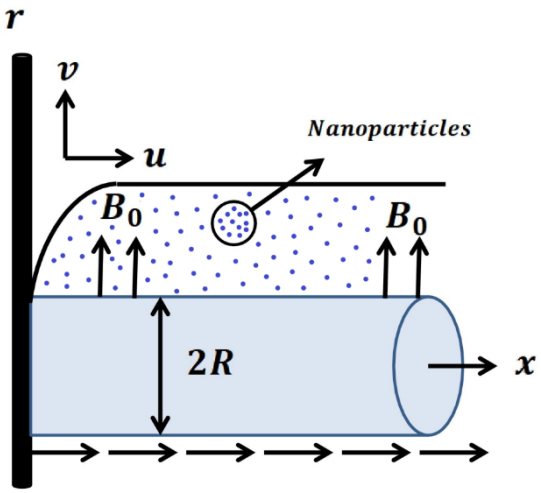

Figure 1 Physical model of problem.

subject to the boundary condition:

$$f_\alpha(0)=0,\quad f_\alpha^{'}(0)=1,\quad \theta_\alpha^{'}(0)=-\beta_1\left(1-\theta_\alpha(0)\right),\quad \phi_\alpha^{'}(0)=-\beta_2\left(1-\phi_\alpha(0)\right)$$
$$f_\alpha^{'}(\xi)\to 0,\quad \theta_\alpha(\xi)\to 0,\quad \phi_\alpha(\xi)\to 0\quad as\quad \xi\to\infty \tag{5}$$

Various fluid parameters are given by:

$$Pr=\frac{\nu}{\alpha},\ Le=\frac{\alpha}{D_B},\ Nt=\frac{(\rho c)_p D_T(T_f-T_\infty)}{(\rho c)_f T_\infty \nu},\ Nb=\frac{(\rho c)_p D_B(C_w-C_\infty)}{(\rho c)_f \nu},\ A=\frac{\alpha_1 L}{c}$$
$$Q=\frac{Q_0 L}{c(\rho c)_f},\ Rd=\frac{4\sigma^* T_\infty^3}{kk^*},\ M=\frac{\sigma {B_0}^2 L}{\rho c},\ \beta_1=\frac{h_f}{k}\sqrt{\frac{\nu L}{c}},\ \beta_2=\frac{k_m}{D_m}\sqrt{\frac{\nu L}{c}} \tag{6}$$

Physical quantities of interest i.e. C_f, Nu_x and Sh_x are described as:

$$C_f=\frac{\tau_w}{\rho U_\infty^2},\ Nu_x=\frac{xq_w}{k(T_f-T_\infty)},\ Sh_x=\frac{xq_m}{D_B(C_w-C_\infty)}, \tag{7}$$

Where:

$$\tau_w=\mu\left(1+\frac{1}{\beta}\right)\left(\frac{\partial u}{\partial r}\right)_{r=R},\ q_w=-\left(\alpha+\frac{16\sigma^* T_\infty^3}{3(\rho c)_f k^*}\right)\left(\frac{\partial T}{\partial r}\right)_{r=R},\ q_m=-D_B\left(\frac{\partial T}{\partial r}\right)_{r=R}, \tag{8}$$

where μ is the dynamic viscosity of nanofluid.
Thus:

$$C_f Re_x^{1/2}=\left(1+\frac{1}{\beta}\right)f_\alpha^{''}(0),\ Nu_x Re_x^{-1/2}=-\left(1+\frac{4}{3}Rd\right)\theta_\alpha^{'}(0),\ Sh_x Re_x^{-1/2}=-\phi_\alpha^{'}(0), \tag{9}$$

where $Re_x=U_\infty x/\nu$ is the local Reynolds number.

Numerical scheme

The nature of D.E's (8) - (10) are non-linear and due to non-linear behavior, these are not solved analytically. Thusly, a numerical technique especially Runge Kutta Fehlberg technique has been carried out to get proper solutions by using MATLAB programming**.** Additionally, inbuilt ODE45 solver is used by following shooting procedure. The whole numerical solution for shooting method works as displayed in **Figure 2** (Flow chart). Re-arranged D.E's (8) - (10) takes the form:

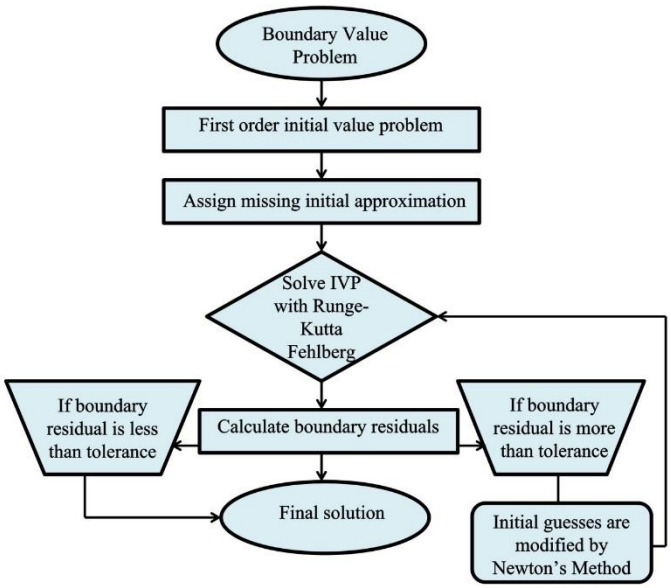

Figure 2 Shooting technique flow chart.

$$f_\alpha''' = \frac{-1}{\left(1+\frac{1}{\beta}\right)(1+2\xi\gamma)}\left[2\gamma\left(1+\frac{1}{\beta}\right)f_\alpha'' + \left(\frac{n+1}{2}\right)f_\alpha f_\alpha'' - n f_\alpha'^{2} - M f_\alpha'\right] \tag{10}$$

$$\theta_\alpha'' = \frac{-1}{(1+2\xi\gamma)\left(1+\frac{4}{3}Rd\right)}\left[\begin{array}{c} PrNb(1+2\xi\gamma)\theta_\alpha'\phi_\alpha' + PrNt(1+2\xi\gamma)\theta_\alpha'^{2} + PrQ\theta_\alpha \\ 2\gamma\left(1+\frac{4}{3}Rd\right)\theta_\alpha' + Pr\left(\frac{n+1}{2}\right)f_\alpha\theta_\alpha' \end{array}\right] \tag{11}$$

$$\phi_\alpha'' = \frac{-1}{(1+2\xi\gamma)}\left[\left(\frac{n+1}{2}\right)LePrf_\alpha\,\phi_\alpha' + 2\gamma\phi_\alpha' + (1+2\xi\gamma)\frac{Nt}{Nb}\theta_\alpha'' - LePrA\phi_\alpha + 2\gamma\frac{Nt}{Nb}\theta_\alpha'\right] \tag{12}$$

New set of variables are defined to get O.D.E's of first order:

$$f_\alpha = s_1,\quad f_\alpha' = s_2,\quad f_\alpha'' = s_3,\quad \theta_\alpha = s_4,\quad \theta_\alpha' = s_5,\quad \phi_\alpha = s_6,\quad \phi_\alpha' = s_7 \tag{13}$$

Coupled system of D.E's are converted into (20) - (26) by using Eq. (19):

$$s_1' = s_2 \tag{14}$$

$$s_2^{'} = s_3 \tag{15}$$

$$s_3^{'} = \frac{-1}{\left(1+\frac{1}{\beta}\right)\left(1+2\xi\gamma\right)}\left[2\gamma\left(1+\frac{1}{\beta}\right)s_3 + \left(\frac{n+1}{2}\right)s_1 s_3 - n s_2^2 - M s_2\right] \tag{16}$$

$$s_4^{'} = s_5 \tag{17}$$

$$s_5^{'} = \frac{-1}{\left(1+2\xi\gamma\right)\left(1+\frac{4}{3}Rd\right)}\left[\begin{array}{c} PrNb\left(1+2\xi\gamma\right)s_5 s_7 + PrNt\left(1+2\xi\gamma\right)s_5^2 + \Pr Q s_4 \\ 2\gamma\left(1+\frac{4}{3}Rd\right)s_5 + Pr\left(\frac{n+1}{2}\right)s_1 s_5 \end{array}\right] \tag{18}$$

$$s_6^{'} = s_7 \tag{19}$$

$$s_7^{'} = \frac{-1}{\left(1+2\xi\gamma\right)}\left[\left(\frac{n+1}{2}\right)Le\Pr s_1 s_7 + 2\gamma s_7 + \left(1+2\xi\gamma\right)\frac{Nt}{Nb}s_5^{'} - Le\Pr A s_6 + 2\gamma\frac{Nt}{Nb}s_5\right] \tag{20}$$

The relevant boundary conditions are reduced to:

$$\begin{array}{c} s_1\left(\xi\right)=0, s_2\left(\xi\right)=1, s_4\left(\xi\right)=-\beta_1\left(1-s_4\left(\xi\right)\right), s_6\left(\xi\right)=-\beta_2\left(1-s_6\left(\xi\right)\right) \quad \text{at} \quad \xi=0 \\ \text{and} \quad s_2\left(\xi\right)=0, s_6\left(\xi\right)=0, s_4\left(\xi\right)=0 \quad \text{as} \quad \xi\to\infty \end{array} \tag{21}$$

Validation of numerical scheme

Resulting outcomes for local Nusselt number are correlates by results of Pal *et al*. [8], Gorla and Sidawi [35] and Kandasamy *et al*. [9] for different Pr by following shooting procedure with fixed controlling fluid parametric values as $n=1, d=0, Sc=1, Nb=Nt=0 \text{and} M=0$ can be visualized in **Table 1**. Moreover for non-linear stretching cylinder, results for $-\theta_\alpha^{'}(0)$ are compared with Rana and Bhargava [21] and Cortell [22] for various entries of n and Pr by taking Nt and Nb zero**. Figures 3 - 5** consequently represents the bar graphs showing comparison of $-\theta_\alpha^{'}(0)$ for stretching cylinder in linear and non-linear cases.

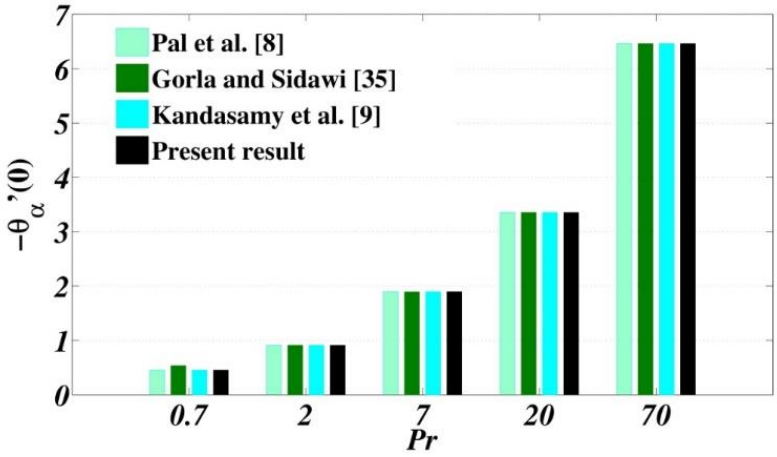

Figure 3 Bar graph showing comparison of local Nusselt number $-\theta_\alpha'(0)$ for linear stretching cylinder.

Table 1 Comparison of results for $-\theta_\alpha'(0)$ for linear case with fixed entries $M=0, Sc=1, Nt=Nb=0$.

Pr	Pal *et al.* [8]	Gorla and Sidawi [35]	Kandasamy *et al.* [9]	Present work
0.7	0.4539	0.5349	0.4542	0.4545
2	0.9113	0.9113	0.9114	0.9114
7	1.8954	1.8905	1.8952	1.8955
20	3.3539	3.3539	3.3538	3.3538
70	6.4622	6.4622	6.4621	6.4622

Table 2 Values for local Nusselt number $-\theta_\alpha'(0)$ for non-linear case when $Nt=Nb=0$, a comparison for different values of n and Pr.

Pr	*n*	Rana and Bhargava [21]	Cortell [22]	Present results
1.0	0.1	0.6101	0.6102	0.6103
	0.5	0.5955	0.5952	0.5953
	1.5	0.5756	0.5745	0.5748
	3.0	0.5660	0.5644	0.5648
5.0	0.1	1.5683	1.6071	1.6078
	0.5	1.5512	1.5867	1.5868
	1.5	1.5269	1.5574	1.5577
	3.0	1.5144	1.5423	1.5432

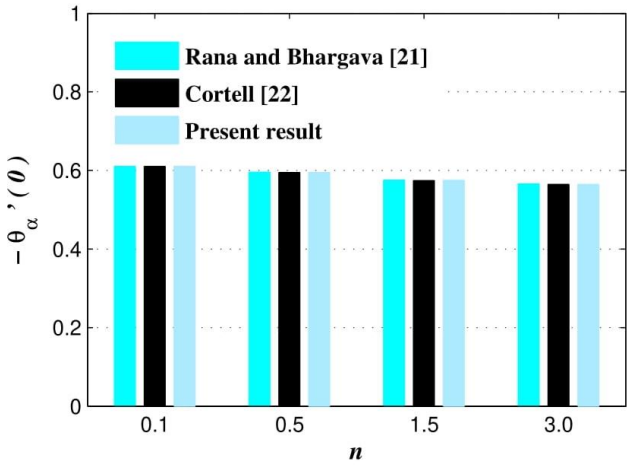

Figure 4 Bar graph showing comparison of local Nusselt number $-\theta_\alpha'(0)$ for non-linear stretching cylinder when $Pr = 1.0$.

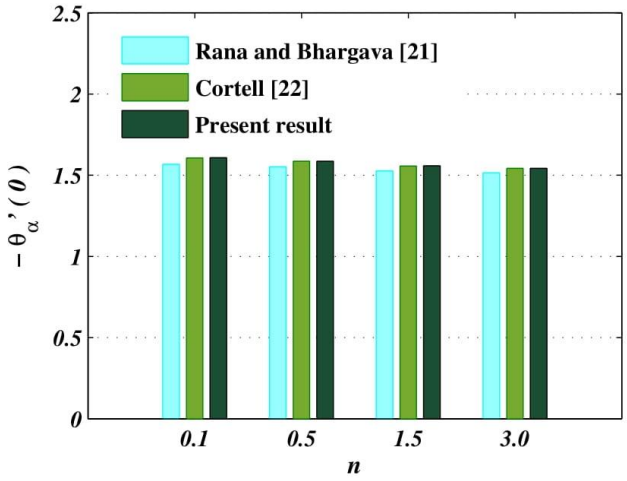

Figure 5 Bar graph showing comparison of local Nusselt number $-\theta_\alpha'(0)$ for non-linear stretching cylinder when $Pr = 5.0$.

Results and discussion

In current analysis, D.E's (8) - (10) along with B.C's (11) are solved by numerical technique (RKF) in MATLAB using ODE45 solver. Results are calculated for controlling parameters especially $\beta, Rd, A, Nt, Nb, \beta_2, \beta_1$ and M on $f_\alpha'(0), \theta_\alpha(0)$ and $\phi_\alpha(0)$. Fixed values of controlling fluid parameters are taken as $\beta = 0.10$, $Nb = 0.1$, $Nt = 0.3$, $A = 0.2$, $M = 2.0$, $\beta_1 = 0.5$, $\beta_2 = 0.1$, $Pr = 5.0$ and $Rd = 0.5$. Table 3 demonstrates the impact of fluid parameters β, Nb, A and M on $f_\alpha'(0), \theta_\alpha(0)$ and $\phi_\alpha(0)$ when $Pr = 5.0$, $Rd = \beta_1 = 0.5$ and $\beta_2 = 0.1$.

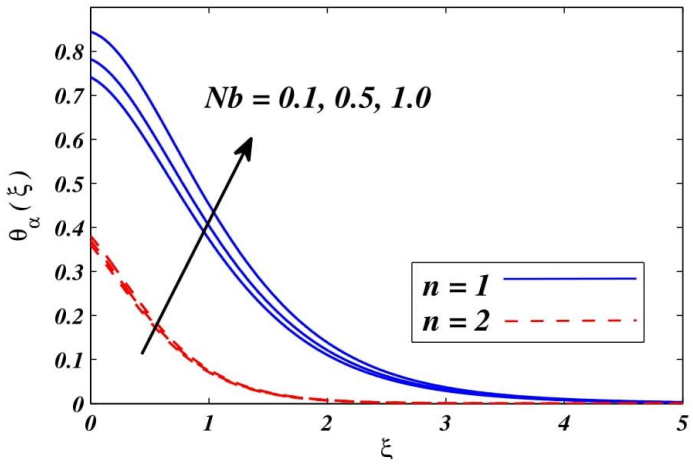

Figure 6 Temperature $\theta_\alpha(\xi)$ for precised entries of Nb for 2 distinct cases of n i.e. for $n=1$ and $n=2$.

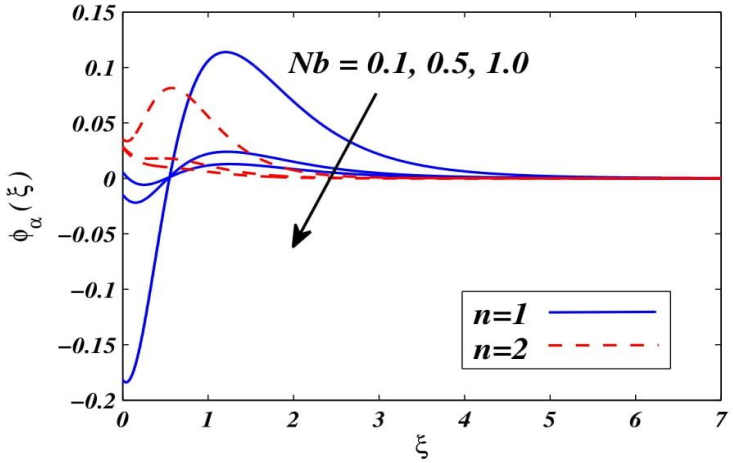

Figure 7 Concentration $\phi_\alpha(\xi)$ for precised entries of Nb for 2 distinct cases of n i.e. for $n=1$ and $n=2$.

Figure 6 examines significance of nanofluid parameter $Nb(0.1,0.5,1.0)$ for linear and non-linear cases of stretching cylinder over temperature field. Physically, an arbitrary motion is produced when fluid particles colloid with each other and this is known as Brownian motion which consequently intensifies width of boundary layer. Therefore, higher Nb increases temperature for both values of n (i.e. for $n=1$ and $n=2$) and elevates values of local Nusselt number as seen in **Table 3**.

Figure 7 manifests the impact of $Nb(0.1,0.5,1.0)$ on concentration $\phi_\alpha(\xi)$ for 2 distinct values of n. Augmentation in value of Nb falls down nanoparticle concentration due to higher collision of fluid particles for both n. Additionally, meets a very good convergence criterion at $\xi=4.5$ (approximately). Moreover, reduction in $-\phi_\alpha'(0)$ has been observed for greater Nb as shown in **Table 3**.

Table 3 Values of $f_\alpha^{''}(0)$, $-\theta_\alpha^{'}(0)$ and $-\phi_\alpha^{'}(0)$ for 2 distinct cases of non-linear stretching parameter n i.e. for $n=1$ (Linear case) and $n=2$ (Non-linear case) when $\beta_1=0.5$, $\beta_2=0.1$, $Pr=5.0$ and $Rd=0.5$.

β	Nb	Nt	A	M	$n=1$(Linear Case)			$n=2$(Non-Linear Case)		
					$f_\alpha^{''}(0)$	$-\theta_\alpha^{'}(0)$	$-\phi_\alpha^{'}(0)$	$f_\alpha^{''}(0)$	$-\theta_\alpha^{'}(0)$	$-\phi_\alpha^{'}(0)$
0.10	0.1	0.3	0.2	2.0	−0.65601	0.12931	0.11816	−0.71993	0.31950	0.09641
0.11					−0.67849	0.08305	0.12333	−0.74554	0.31789	0.09651
0.12					−0.69980	0.03290	0.12902	−0.76978	0.31631	0.09661
0.10	0.1				−0.65601	0.12931	0.11816	−0.71993	0.31950	0.09641
	0.5				−0.65601	0.10883	0.10146	−0.71993	0.31518	0.09711
	1.0				−0.65601	0.07768	0.09943	−0.71993	0.30965	0.09720
	0.1	0.1			−0.65601	0.23037	0.09974	−0.71993	0.33609	0.09611
		0.2			−0.65601	0.19639	0.10569	−0.71993	0.32825	0.09585
		0.3			−0.65601	0.12931	0.11816	−0.71993	0.31950	0.09641
		0.3	0.0		−0.65601	0.12351	0.22905	−0.71993	0.31796	0.18339
			0.5		−0.65601	0.11977	0.22843	−0.71993	0.31894	0.19178
			1.0		−0.65601	0.11067	0.22419	−0.71993	0.31922	0.19527
			0.2	0.0	−0.45010	0.23373	0.10677	−0.54007	0.32947	0.09582
				1.0	−0.56239	0.19856	0.11053	−0.63655	0.32445	0.09610
				2.0	−0.65601	0.12931	0.11816	−0.71993	0.31950	0.09641

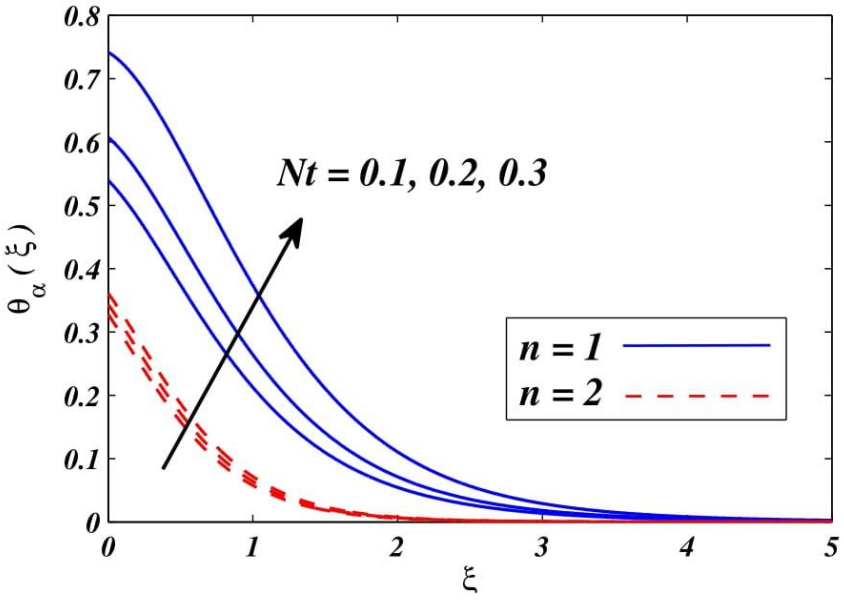

Figure 8 Temperature $\theta_\alpha(\xi)$ for precised entries of Nt for 2 distinct cases of n i.e. for $n=1$ and $n=2$.

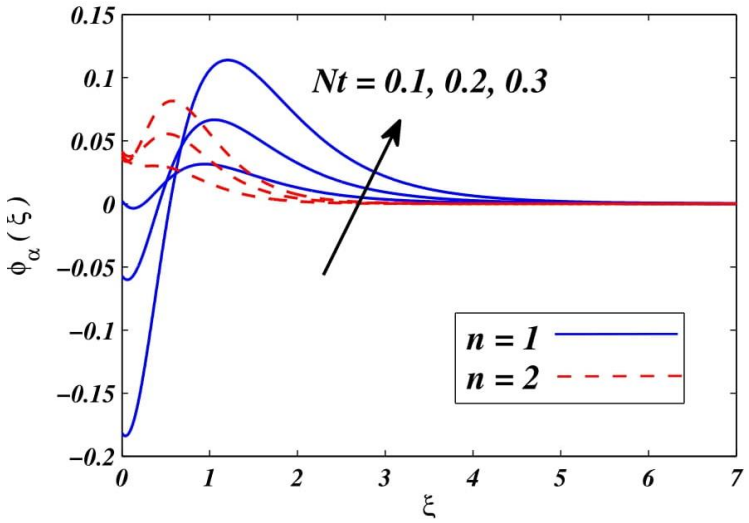

Figure 9 Concentration $\phi_\alpha(\xi)$ for precised entries of Nt for 2 distinct cases of n i.e. for $n=1$ and $n=2$.

Figure 8 deliberates consequence of thermophoresis Nt over temperature field for $n=1$ and $n=2$. Temperature gradient tumbles down for higher thermophoresis Nt to such an extent that a decrease in pace of conduction of nanoparticles is noticed**.** Along these lines, width of boundary layer upgrades and thus, temperature improves with higher Nt for the 2 upsides of non-linear extending parameter n.

Figure 9 portraits variation in $\phi_\alpha(\xi)$ against $Nt(0.1,\ 0.2,\ 0.3)$. This diagram manifests that expansion in Nt upgrades concentration of nanoparticles. Fundamentally, in the event of thermophoretic force applied by a molecule on the other molecule will produces the development of particles from hotter locale to cold locale and henceforth strengthening in nanoparticle concentration is noticed through **Figure 9**.

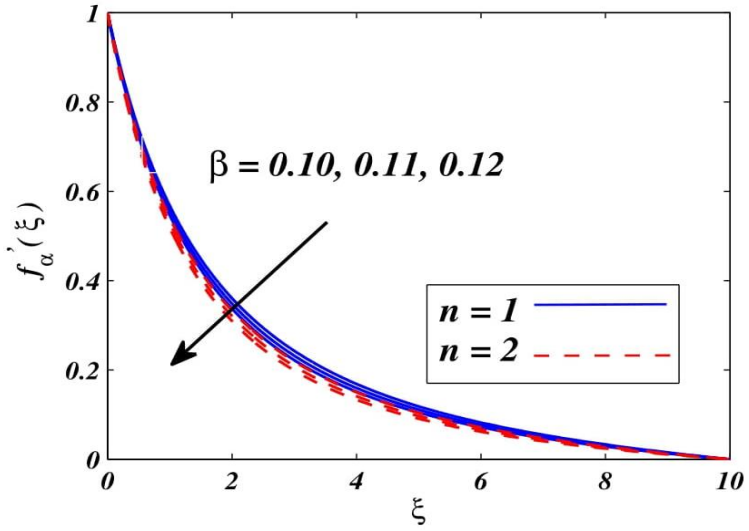

Figure 10 Velocity $f'_\alpha(\xi)$ for precised entries of β for 2 distinct cases of n i.e. for $n=1$ and $n=2$.

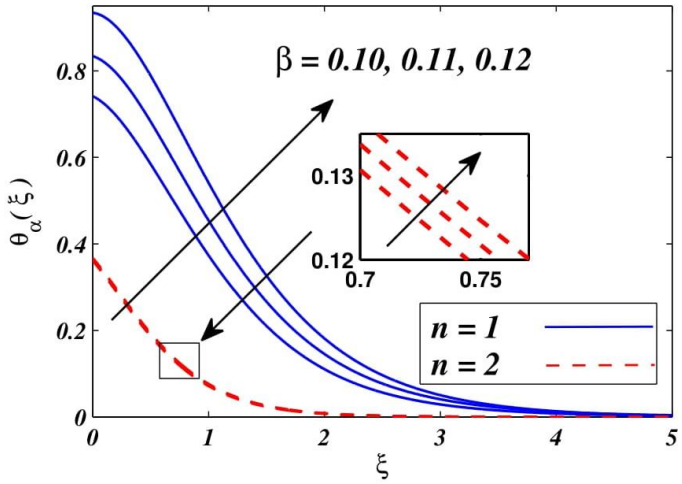

Figure 11 Temperature $\theta_\alpha(\xi)$ for precised entries of β for 2 distinct cases of n i.e. for $n=1$ and $n=2$.

Velocity profile $f_\alpha^{'}(\xi)$ variation against Casson fluid parameter $\beta(0.10,0.11,0.12)$ for respective values of $n=1$ and $n\neq 1$ has been illustrated via **Figure 10**. A decrease in velocity profile is noticed for higher Casson fluid parameter β. This graph elaborates that enhancement in the value of β will declines yield stress that hurdles the free movement of fluid particles and hence boundary layer thickness reduces. Thus, fluid velocity decreases for both values of n. Consequently, the decay in the value of skin friction coefficient is observed in **Table 3**. **Figure 11** depicts the behavior of $\beta(0.10,0.11,0.12)$ on temperature distribution $\theta_\alpha(\xi)$. This figure indicates that as Casson fluid parameter β increases, fluid temperature enhances and this graph elaborates that enhancement in the value of β enhances fluid velocity that will intensify the heat transfer rate. Hence fluid temperature rises due to the presence of n. Additionally, a very slight increase in temperature is noticed for $n=2$ that is fluid temperature enhances with higher speed in case of the stretching cylinder in a non-linear way as seen in Figure 11**.** Consequently, decay in Nu_x is noticed in **Table 3**. **Table 4** demonstrates the impact of fluid parameters β_1, β_2, Pr and Rd on $f_\alpha^{''}(0)$, $-\theta_\alpha^{'}(0)$ and $-\phi_\alpha^{'}(0)$ by taking fixed entries of other fluid parameters namely Casson fluid parameter β as 0.10, thermophoresis parameter Nt as 0.3, chemical reaction parameter A as 0.2, magnetic parameter M as 2.0 and Brownian motion Nb as 0.1.

Table 4 Values of $f_\alpha^{''}(0)$, $-\theta_\alpha^{'}(0)$ and $-\phi_\alpha^{'}(0)$ for 2 distinct cases of non-linear stretching parameter n i.e. for $n=1$ (Linear case) and $n=2$ (Non-linear case) when $\beta=0.10$, $Nb=0.1$, $Nt=0.3$, $M=2.0$ and $A=0.2$.

β_1	β_2	Pr	Rd	$n=1$(Linear Case)			$n=2$(Non-Linear Case)		
				$f_\alpha^{''}(0)$	$-\theta_\alpha^{'}(0)$	$-\phi_\alpha^{'}(0)$	$f_\alpha^{''}(0)$	$-\theta_\alpha^{'}(0)$	$-\phi_\alpha^{'}(0)$
0.5	0.10	5.0	0.5	−0.65601	0.19639	0.10569	−0.71993	0.32825	0.09585
1.0				−0.65601	0.21260	0.10968	−0.71993	0.47069	0.09635
1.5				−0.65601	0.21385	0.11137	−0.71993	0.54376	0.09695
0.5	0.10			−0.65601	0.19639	0.10569	−0.71993	0.32825	0.09585
	0.15			−0.65601	0.19505	0.15611	−0.71993	0.32778	0.14180

β_1	β_2	Pr	Rd	$n=1$(Linear Case)			$n=2$(Non-Linear Case)		
				$f_\alpha''(0)$	$-\theta_\alpha'(0)$	$-\phi_\alpha'(0)$	$f_\alpha''(0)$	$-\theta_\alpha'(0)$	$-\phi_\alpha'(0)$
	0.20			−0.65601	0.19375	0.20501	−0.71993	0.32732	0.18652
	0.10	3.0		−0.65597	0.08280	0.12180	−0.71993	0.28591	0.09556
		5.0		−0.65601	0.12931	0.11816	−0.71993	0.31950	0.09641
		7.0		−0.65601	0.16059	0.11634	−0.71993	0.33614	0.09733
		5.0	1.0	−0.65600	0.02786	0.12346	−0.71993	0.29873	0.09715
			2.0	−0.65597	0.19018	0.10479	−0.71993	0.26084	0.09842
			3.0	−0.65582	0.19653	0.10257	−0.71993	0.22482	0.09950

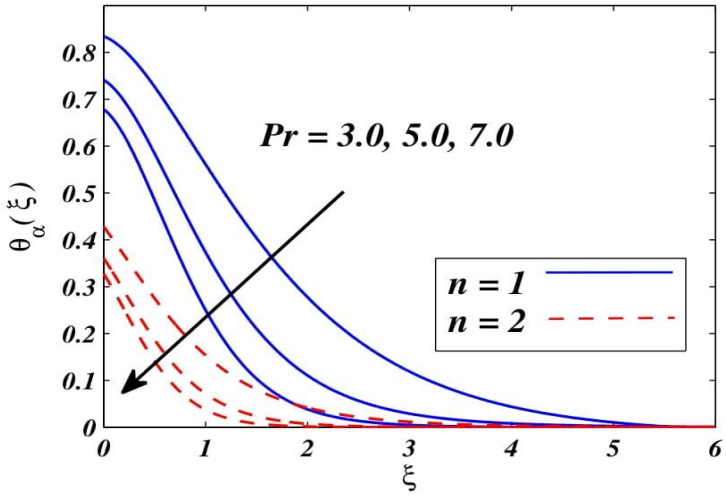

Figure 12 Temperature $\theta_\alpha(\xi)$ for precised entries of Pr for 2 distinct cases of n i.e. for $n=1$ and $n=2$.

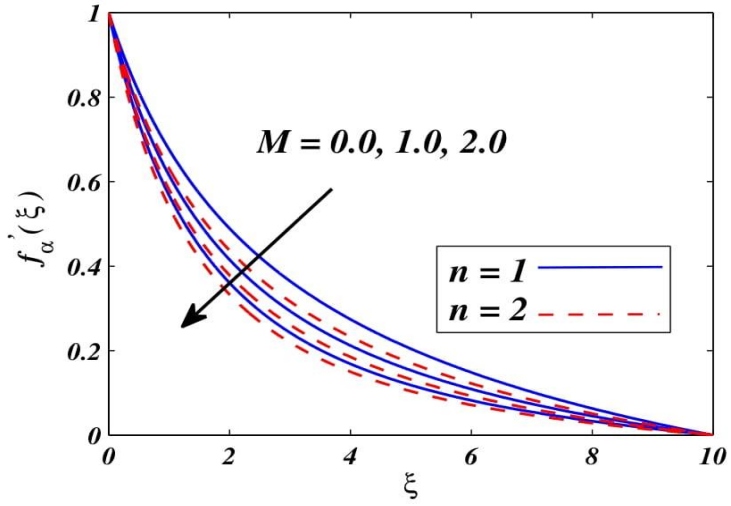

Figure 13 Velocity $f_\alpha'(\xi)$ for precised entries of M for 2 distinct cases of n i.e. for $n=1$ and $n=2$.

Prandtl number is the "dimensionless" quantity and is the ratio of momentum diffusivity to the thermal diffusivity. If relatively higher viscous fluid is taken then Pr increases and there is less convection in heat transfer rate. variation in temperature distribution against Prandtl number is displayed through the **Figure 12** for $n=1$ and $n=2$. As the value of Pr increases it will reduce the thermal diffusivity. Low thermal diffusivity decreases the thickness of temperature and boundary thickness as illustrated in **Figure 12**. **Figure 13** manifests magnetic field impact against velocity distribution with variation in values of n. This figure illustrates that magnetic field existence opposes the liquid molecule to move unreservedly and principle purpose for the opposition is that M produces Lorentz drag force and this attraction conduct can be embraced for controlling the smooth motion of the fluid**.** Consequently an improvement in M causes the rot of speed circulation as portrayed by means of **Figure 13**.

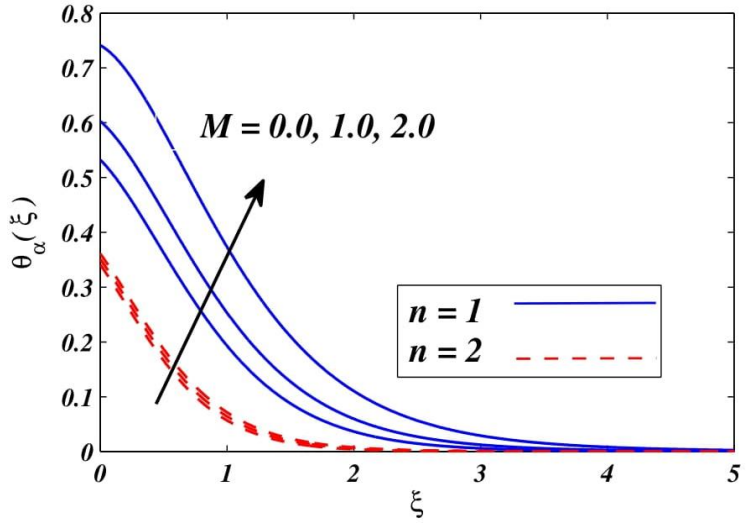

Figure 14 Temperature $\theta_\alpha(\xi)$ for precised entries of M for 2 distinct cases of n i.e. for $n=1$ and $n=2$.

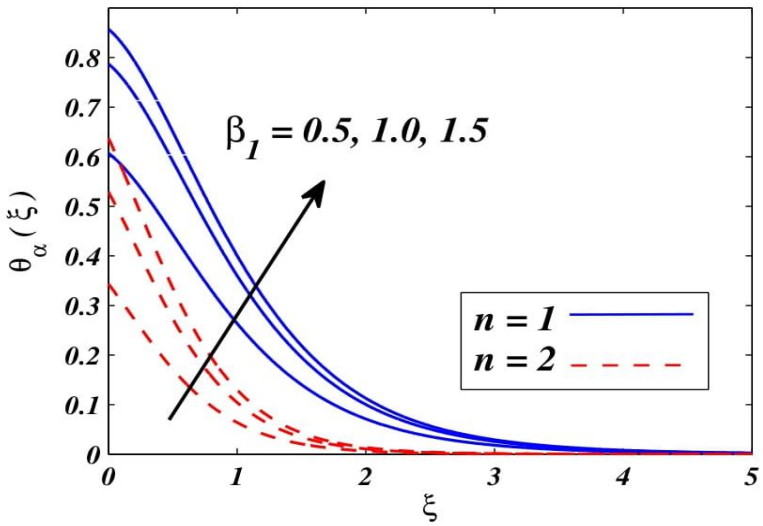

Figure 15 Temperature $\theta_\alpha(\xi)$ for precised entries of β_1 for 2 distinct cases of n i.e. for $n=1$ and $n=2$.

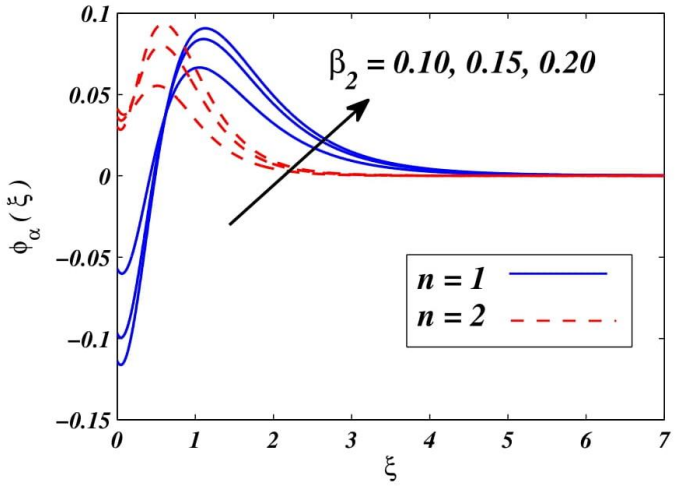

Figure 16 Concentration $\phi_\alpha(\xi)$ for precised entries of β_2 for 2 distinct cases of n i.e. for $n=1$ and $n=2$.

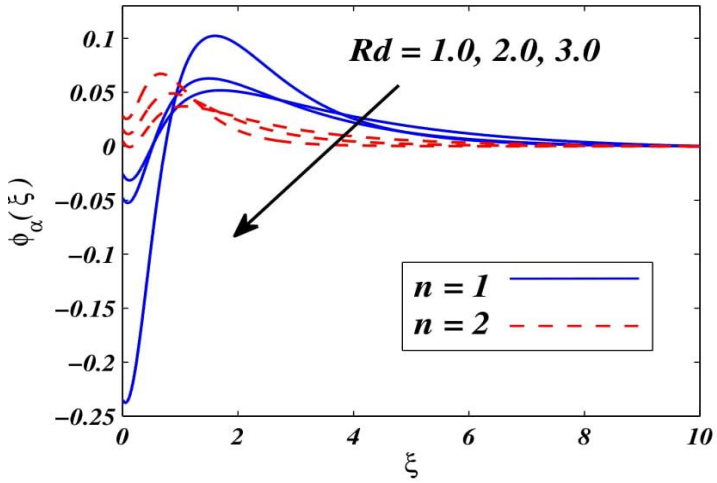

Figure 17 Concentration $\phi_\alpha(\xi)$ for precised entries of Rd for 2 distinct cases of n i.e. for $n=1$ and $n=2$.

Figure 14 reflects influence of crucial magnetic parameter $M\,(0.0 \le M \le 2.0)$ over temperature distribution for 2 distinct cases of stretching cylinder in linear $(n=1)$ and non-linear $(n \ne 1)$ way. With an increase in M, the velocity distribution diminishes as a result of fabrication of Lorentz force that thusly heighten the heat transportation rate and boundary layer thickness**.** Thus temperature field intensifies for both values of n as shown graphically.

Figure 15 elucidates variation of temperature under the influence of thermal Biot number $\beta_1\,(0.5,1.0,1.5)$ for 2 values of n. As thermal Biot number β_1 enhances, fluid temperature also enhances. Higher β_1 rises the value of heat transportation coefficient that results in intensification of boundary layer thickness and temperature for both n **(**i.e. for $n=1 \& n=2$**)** and consequently Nusselt number reduces as shown in **Table 4**.

Figure 16 represents variation of concentration under the impact of $\beta_2\,(0.10, 0.15, 0.20)$. **Figure 16** shows that as value of β_2 increases, concentration profile also increases for both n. **Figure 17** illustrates the profile of nanoparticle concentration for radiation parameter $Rd\,(1.0, 2.0, 3.0)$. This plot elucidates that with increase in $Rd\,(1.0 \le Rd \le 3.0)$, mean absorption coefficient decreases that increase the fluid temperature and consequently increases nanoparticle concentration $\phi_\alpha(\xi)$.

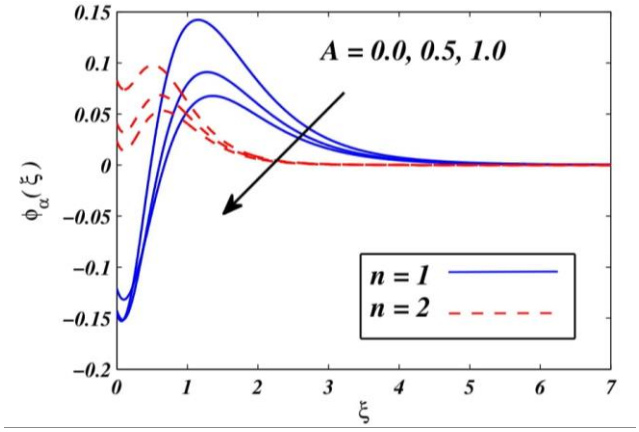

Figure 18 Concentration $\phi_\alpha(\xi)$ for precised entries of A for 2 distinct cases of n i.e. for $n=1$ and $n=2$.

Figure 18 illustrates nanoparticle concentration against chemical reaction parameter $A\,(0.0, 0.5, 1.0)$. Chemical reaction facilitates in consumption of chemically reacting particles that results in reduction of concentration. This is the major cause of fall in concentration with rise in chemical reaction parameter A for both cases of non-linear stretching parameter n as depicted in **Figure 18**.

Figure 19 deliberates the variation of $C_f Re_x^{1/2}$ for precised entries of β, $M\,(0.0, 1.0, 2.0)$ and $n\,(1, 2)$. This graph elaborates that higher β decline skin friction coefficient value. Principle purpose for the decrease in skin friction coefficient is the presence of Casson fluid β which decays dimensionless velocity because of which velocity gradient increments. Also skin friction coefficient is higher for linear case (i.e. for $n=1$) of stretching cylinder when compared to non-linear situation (i.e. for $n \neq 1$). Moreover skin friction coefficient declines monotonically for greater magnetic parameter M.

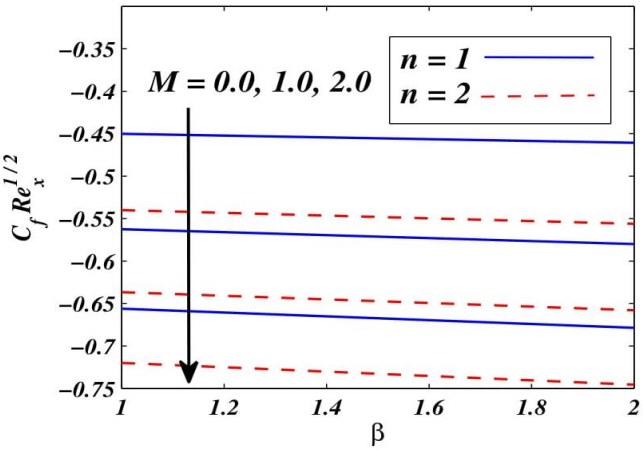

Figure 19 Skin friction coefficient $C_f Re_x^{1/2}$ for precised entries of M and β for 2 distinct cases of n i.e. for $n=1$ and $n=2$.

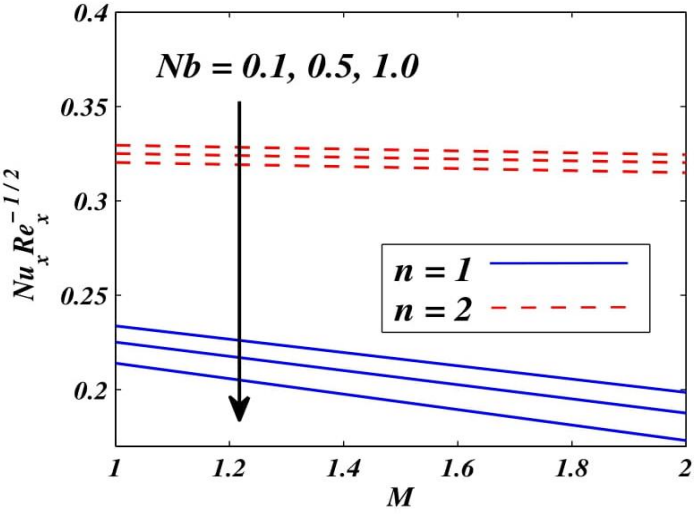

Figure 20 Local Nusselt number $Nu_x Re_x^{-1/2}$ for precised entries of M and Nb for 2 distinct cases of n i.e. for $n=1$ and $n=2$.

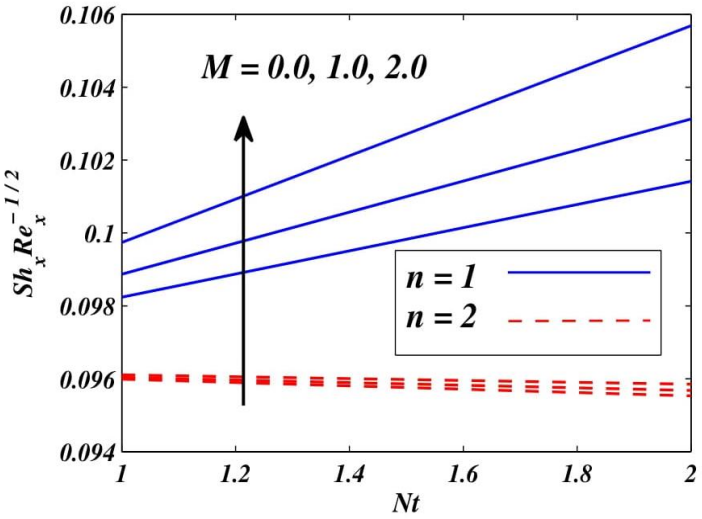

Figure 21 Local Sherwood number $Sh_x Re_x^{-1/2}$ for precised entries of M and Nt for 2 distinct cases of n i.e. for $n=1$ and $n=2$.

Figure 20 manifests the rate of heat transportation against M, $Nb(0.1 \le Nb \le 1.0)$ and n (1,2). This graph shows that as the value of fluid parameters Brownian motion Nb and magnetic M intensifies, heat transportation rate declines for both values of n. On the other hand, local Nusselt number is higher for non-linearity in comparison to linearity of stretching parameter n.

Figures 21 illustrates the impact of fluid parameter $M(0.0 \le M \le 2.0)$, Nt and n (1,2) over rate of mass transportation. With intensification in magnetic M, Sherwood number enhances and opposite behavior is noticed for rate of mass transportation in case of thermophoresis Nt. As Nt increases then Sherwood number rises for linear stretching parameter (i.e. linear case, $n=1$) while it slightly declines for non-linear stretching parameter (i.e. non-linear case, $n=2$).

Conclusions

MHD Casson fluid flow with chemical reacting nanoparticles and convective boundary conditions past a linear/non-linear stretching cylinder has been discussed in current research. Present results are compared with Pal *et al*. [8], Gorla and Sidawi [35] and Kandasamy *et al*. [9] for linear case and with Rana and Bhargava [21] and Cortell [22] for non-linear case. Velocity, nanoparticle concentration, temperature field and physical quantities of interest are taken into account for controlling parameters β, M, A, β_1, β_2, Rd and Pr for different n. Main results are as follows:

1) Declination in velocity is observed for greater Casson fluid β and magnetic parameter M. Additionally, in both these fluid parameters β and M, velocity profile is greater for stretching cylinder in linear $(n+1)$ way when compared to the non-linear case $(n+2)$.

2) Intensification in temperature field is noticed for crucial parameters especially thermophoresis Nt, Brownian motion Nb, Casson fluid β, magnetic M and thermal Biot number β_1. However temperature declines due to lower thermal conductivity for higher value of Prandtl number Pr for both linear and non-linear cases.

3) Nanoparticle concentration elevates for controlling fluid parameters namely chemical reaction A, radiation Rd and Brownian motion Nb whereas nanoparticle concentration intensifies for higher concentration Biot number β_2 and thermophoresis Nt.

4) Augmentation in M will elevated the skin friction coefficient value due to Lorentz drag force which consequently enhances $-\theta'_\alpha(0)$ and $-\phi'_\alpha(0)$ that helps in the heat transfer rate controlling.

Nomenclature

x, y	Cartesian coordinates
C_w	Nanoparticle volume fraction (Kg.m^{-3})
C	Concentration (Kg.m^{-3})
L	Characteristic length
Le	Lewis number
c	Positive constant
q_m	Surface mass flux $(\mathrm{W.m^{-2}})$
B	Magnetic field strength **(**Tesla**)**
Nu_x	Nusselt number
Nt	Thermophoresis parameter
M	Magnetic field parameter **(**Tesla**)**
u	Horizontal velocity $(\mathrm{m.s^{-1}})$
C_∞	Ambient nanoparticle volume fraction (Kg.m^{-3})
q_w	Surface heat flux $(\mathrm{W.m^{-2}})$
T_w	Temperature at the sheet **(**K**)**
D_T	Thermophoresis diffusion coefficient $(\mathrm{m^2.s^{-1}})$
u_w	Stretching velocity $(\mathrm{m.s^{-1}})$
T	Temperature **(**K**)**
Nb	Brownian motion parameter
D_B	Brownian diffusion coefficient $(\mathrm{m^2.s^{-1}})$

v	Vertical velocity $(\mathrm{m.s^{-1}})$
Sh_x	Sherwood number
Pr	Prandtl number
T_∞	Ambient temperature **(**K**)**

Greek Symbols

ν	Kinematic viscosity $(\mathrm{m^2.s^{-1}})$
β	Casson fluid parameter
β_2	Concentration Biot number
σ	Electrical conductivity
ξ	Similarity variable
ρ_f	Density of base fluid ($\mathrm{Kg.m^{-3}}$)
ϕ_α	Non-dimensional concentration
θ_α	Non-dimensional temperature
τ	Ratio of heat capacities
α	Thermal diffusivity $(\mathrm{m^2.s^{-1}})$
β_1	Thermal Biot number

Subscripts

p	Particle
∞	Ambient condition
f	Fluid
w	Wall

Superscripts

'	Prime denotes derivative w.r.t to ξ

Acknowledgements

Author's wishing to express their cordial thanks to Mr. Madan Lal Makkar and Mrs. Neelam Makkar for their love, support and constant encouragement throughout the study.

References

[1] BC Sakiadis. Boundary-layer behavior on continuous solid surfaces: I. Boundary-layer equations for two-dimensional and axisymmetric flow. *AIChE J.* 1961; **7**, 26-8.
[2] LJ Crane. Flow past a stretching plate. *Z. Angew. Math. Phys.* 1970; **21**, 645-7.
[3] SUS Choi and JA Eastman. Enhancing thermal conductivity of fluids with nanoparticles. *In*: Proceedings of the 1995 International mechanical engineering congress and exhibition, California. 1995, p. 12-7.
[4] Y Xuan and Q Li. Heat transfer enhancement of nanofluids. *Int. J. Heat Fluid Flow* 2000; 21, 58-64.
[5] J Buongiorno. Convective transport in nanofluids. *J. Fluid Flow Heat Mass Tran.* 2006; **128**, 240-50.
[6] A Kuznetsov and D Nield. Natural convective boundary-layer flow of a nanofluid past a vertical plate. *Int. J. Therm. Sci.* 2010; **49**, 243-7.
[7] S Nadeem, R Mehmood and NS Akbar. Optimized analytical solution for oblique flow of a Casson-nano fluid with convective boundary conditions. *Int. J. Therm. Sci.* 2014; **78**, 90-100.

[8] D Pal, N Roy and K Vajravelu. Effects of thermal radiation and ohmic dissipation on MHD casson nanofluid flow over a vertical non-linear stretching surface using scaling group transformation. *Int. J. Mech. Sci.* 2016; **114**, 257-67.
[9] R Kandasamy, P Loganathan and PP Arasu. Scaling group transformation for MHD boundarylayer flow of a nanofluid past a vertical stretching surface in the presence of suction/injection. *Nucl. Eng. Des.* 2011; **241**, 2053-9.
[10] R Goyal, Vinita, N Sharma and R Bhargava. GFEM analysis of MHD nanofluid flow toward a power-law stretching sheet in the presence of thermodiffusive effect along with regression investigation. *Heat Tran.* 2020; **50**, 234-56.
[11] Vinita, V Poply, R Goyal and N Sharma. Analysis of the velocity, thermal, and concentration MHD slip flow over a nonlinear stretching cylinder in the presence of outer velocity. *Heat Tran.* 2021; **50**, 1543-69.
[12] V Poply and R Devi. A two-component modeling for free stream velocity in magnetohydrodynamic nanofluid flow with radiation and chemical reaction over a stretching cylinder. *Heat Trans.* 2021; **50**, 3603-19.
[13] MS Abel and N Mahesha. Heat transfer in MHD viscoelastic fluid flow over a stretching sheet with variable thermal conductivity, non-uniform heat source and radiation. *Appl. Math. Model.* 2008; **32**, 1965-83.
[14] T Hayat, M Qasim and S Mesloub. MHD flow and heat transfer over permeable stretching sheet with slip conditions. *Int. J. Numer. Meth Fluid.* 2011; **66**, 963-75.
[15] V Vinita and V Poply. Impact of outer velocity MHD slip flow and heat transfer of nanofluid past a stretching cylinder. *Mater. Today Proc.* 2020; **26**, 3429-35.
[16] T Salahuddin, A Hussain, MY Malik, M Awais and M Khan. Carreau nanofluid impinging over a stretching cylinder with generalized slip effects: Using finite difference scheme. *Results Phys.* 2017; **7**, 3090-9.
[17] A Mishra and M Kumar. Velocity and thermal slip effects on mhd nanofluid flow past a stretching cylinder with viscous dissipation and joule heating. *SN Appl. Sci.* 2020; **2**, 1350.
[18] V Poply and Vinita. *Analysis of outer velocity and heat transfer of nanofluid past a stretching cylinder with heat generation and radiation*. *In*: P Singh, RK Gupta, K Ray and A Bandyopadhyay (Eds.). Advances in Intelligent Systems and Computing. Springer, Singapore, 2020.
[19] Z Abbas and T Hayat. Stagnation slip flow and heat transfer over a nonlinear stretching sheet. *Numer. Meth. Part. Differ. Equat.* 2011; **27**, 302-14.
[20] K Jabeen, M Mushtaq and RM Akram. Analysis of the MHD boundary layer flow over a nonlinear stretching sheet in a porous medium using semianalytical approaches. *Math. Probl. Eng.* 2020; **2020**, 3012854.
[21] P Rana and R Bhargava. Flow and heat transfer of a nanofluid over a nonlinearly stretching sheet: A numerical study. *Comm. Nonlinear Sci. Numer. Simulat.* 2012; **17**, 212-26.
[22] R Cortell. Viscous flow and heat transfer over a nonlinearly stretching sheet. *Appl. Math. Comput.* 2007; **184**, 864-73.
[23] R Sharma and A Bisht. Numerical study of MHD flow and heat transfer of nanofluid along a nonlinear curved stretching surface. *AIP Proc. Conf.* 2018; **1975**, 030025.
[24] M Imtiaz, H Nazar, T Hayat and A Alsaedi. Soret and dufour effects in the flow of viscous fluid by a curved stretching surface. *Pramana* 2020; **94**, 48.
[25] V Makkar, V Poply, R Goyal and N Sharma. Numerical investigation of mhd casson nanofluid flow towards a non linear stretching sheet in presence of double-diffusive effects along with viscous and ohmic dissipation. *J. Therm. Eng.* 2021; **7**, 1-17.
[26] N Casson. *In rheology of dispersed system*, pergamon press, oxford, 1959.
[27] M Mustafa, T Hayat, I Popand and A Aziz. Unsteady boundary layer flow of a casson fluid due to an impulsively started moving flat plate. *Heat Tran.* 2011; **40**, 563-76.
[28] JA Gbadeyan, EO Titiloye and AT Adeosun. Effect of variable thermal conductivity and viscosity on casson nanofluid flow with convective heating and velocity slip. *Heliyon* 2020; **6**, e03076.
[29] T Hayat, S Asad and A Alsaedi. Flow of casson fluid with nanoparticles. *Appl. Math. Mech.* 2016; **37**, 459-70.
[30] Z Shah, P Kumam and W Deebani. Radiative MHD casson nanofluid flow with activation energy and chemical reaction over past nonlinearly stretching surface through entropy generation. *Sci. Rep.* 2020; **10**, 4402.
[31] PK Kameswaran, S Shaw and P Sibanda. Dual solutions of Casson fluid flow over a stretching or shrinking sheet. *Sadhana* 2014; **39**, 1573-83.

[32] MS Khan, I Karim, LE Ali and A Islam. Unsteady MHD free convection boundary-layer flow of a nanofluid along a stretching sheet with thermal radiation and viscous dissipation effects. *Int. Nano Lett.* 2012; **2**, 24.
[33] AA Afify. The Influence of slip boundary condition on casson nanofluid flow over a stretching sheet in the presence of viscous dissipation and chemical reaction. *Math. Probl. Eng.* 2017; **2017**, 3804751.
[34] M Imtiaz, T Hayat and A Alsaedi. Mixed convection flow of casson nanofluid over a stretching cylinder with convective boundary conditions. *Adv. Powder Tech.* 2016; **27**, 2245-56.
[35] RSR Gorla and I Sidawi. Free convection on a vertical stretching surface with suction and blowing. *Appl. Sci. Res.* 1994; **52**, 247-57.